3-10-1998

The Ultraviolet-Optical Albedo of Broad Emission Line Clouds

Kirk Korista
University of Kentucky

Gary J. Ferland
University of Kentucky, gary@uky.edu

The Ultraviolet-Optical Albedo of Broad Emission Line Clouds

Notes/Citation Information
Published in *The Astrophysical Journal*, v. 495, no. 2, p. 672-679.

Digital Object Identifier (DOI)
http://dx.doi.org/10.1086/305330

THE ASTROPHYSICAL JOURNAL, 495:672–679, 1998 March 10

THE ULTRAVIOLET-OPTICAL ALBEDO OF BROAD EMISSION LINE CLOUDS

KIRK KORISTA
Department of Physics and Astronomy, University of Kentucky, Lexington, KY 40506; Department of Physics, Western Michigan University, Kalamazoo, MI 49008

AND

GARY FERLAND
Department of Physics and Astronomy, University of Kentucky, Lexington, KY 40506
Received 1997 July 23; accepted 1997 October 16

ABSTRACT

We explore the effective UV-optical albedos of a variety of types of broad emission line clouds, as well as their possible effects on the observed spectra of active galactic nuclei (AGNs). An important albedo source in moderately ionized ionization-bounded clouds is that which is due to neutral hydrogen: Rayleigh scattering of continuum photons off the extreme damping wings of Lyα. The photons resulting from this scattering mechanism may contribute significantly to the Lyα emission line, especially in the very broad wings. In addition, line photons emitted near 1200 Å (e.g., N v λ1240) that stream toward the neutral portion of the cloud may be reflected off this Rayleigh scattering mirror, so that they preferentially escape from the illuminated face. Inclusion of this effect can alter predicted emission-line strengths and profiles. In more highly ionized ionization-bounded clouds, Thomson scattering dominates the UV-optical albedo, but this albedo is lessened by the hydrogen gas opacity; these clouds are most reflective on the long-wavelength side of the hydrogen recombination edges. This feature may then alter the shapes of the spectral regions near the recombination edges, e.g., the Balmer jump. We illustrate the effects of gas density and line broadening on the effective albedo. We also discuss the reflection effects of the accretion disk and the "dusty torus." The accretion disk is an effective reflector of UV-optical photons, whether by electron or Rayleigh scattering, and it is possible that we observe a significant fraction of this light from the AGNs in reflection. This effect can alter the emission-line profiles and even destroy emission at the Lyman jump emitted by broad-line clouds. Finally, we discuss the possibility that continuum reflection from broad-line clouds is at least in part responsible for the polarized broad absorption line troughs.

Subject headings: galaxies: Seyfert — line: formation — quasars: emission lines — quasars: general — scattering

1. INTRODUCTION

The presence of "mirrors" in the vicinity of active galactic nuclei (AGNs) has been known for more than a decade, mainly via optical/UV spectropolarimetric observations as well as via X-ray observations. Along some lines of sight, the light from the central continuum source and the broad emission line clouds is blocked from our direct view by the putative molecular torus and reflected by material (warm electrons and dust) lying outside the torus opening. The nuclear emission is observed in polarized light in many Seyfert 2 galaxies (Miller & Antonucci 1983; Antonucci & Miller 1985; Miller & Goodrich 1990; Tran, Miller, & Kay 1992; Goodrich & Miller 1994). The "reflection bump" or "Compton mirror" is the reflection of hard X-rays off some object that covers $\sim 2\pi$ sr of the sky as seen from the hard X-ray source (Lightman & White 1988; Ross & Fabian 1993; Nandra & George 1994; Życki et al. 1994; Poutanen et al. 1996). The accompanying Fe Kα emission line requires high column density gas and is thought to arise in the reflecting gas. This mirror is often taken to be the accretion disk, though Krolik, Madau, & Życki (1994) have also proposed the molecular torus. Observations of broad absorption line QSOs (BAL QSOs) show the troughs to be more polarized than the continuum. It has been inferred that part of the rest-frame UV continuum is observed in reflection and/or is partially screened from view (Glenn, Schmidt, & Foltz 1994; Cohen et al. 1995; Goodrich & Miller 1995; Hines & Wills 1995; Goodrich 1997). Finally, strongly rising polarization shortward of the expected intrinsic Lyman limits in two of the three QSOs observed by Koratkar et al. (1995) led them to propose the reflection of an intrinsic Lyman edge in *emission*.

Here we examine the UV-optical albedo $A_{\rm eff}(\lambda) \equiv F_{\rm refl}(\lambda)/F_{\rm inci}(\lambda)$, of broad emission line clouds with hydrogen ionization fronts (henceforth, ionization-bounded clouds) to demonstrate its possible significance to the observed spectra of AGNs. Here, $F_{\rm inci}(\lambda)$ is the incident AGN continuum flux at the illuminated face of the cloud; $F_{\rm refl}(\lambda)$ is the reflected flux that includes only the incident continuum photons reemitted by the illuminated face of the cloud into 2π sr, i.e., it does not include diffuse continua or line emission. A cartoon of the general situation is shown in Figure 1.

In § 2 we present the calculations of the effective albedo, and in § 3 we discuss the implications of the albedo of the broad-line region (BLR) clouds to the observed spectra of AGNs. Ionization-bounded broad-line clouds have a high albedo near 1200 Å because of Lyα Rayleigh scattering of continuum photons. This reflection could account for a small but significant fraction of the measured Lyα λ1216 equivalent width. This mirror could also alter the transport of those lines emitted near Lyα (e.g., N v λ1240). We comment briefly on some of the implications of the existence of Rayleigh and electron scattering mirrors in the accretion disk. We will also discuss the possible contribution of the broad-line clouds' albedo to the polarized light observed in the troughs of BAL QSOs. For comparison, we

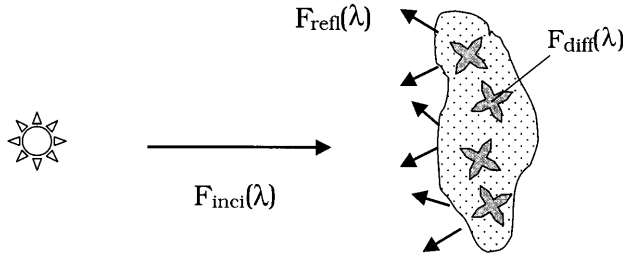

FIG. 1.—Cartoon illustrating the source of continuum photons at left (*star icon*) and a broad emission line cloud at right. Incident and reflected continua and the diffuse emission are labeled. As defined here, the reflected continuum does not include diffuse emission.

will illustrate the albedo of a dusty cloud whose parameters roughly approximate that of the "molecular torus."

2. CALCULATIONS

2.1. *The Effective Albedo: Scattering versus Absorption*

The effective albedo of a cloud is the result of a competition between scattering and absorption. The dominant scattering mechanism in the UV in high column density, high-ionization broad-line clouds is Thomson (electron) scattering, and that in clouds with significant neutral hydrogen column densities is Rayleigh scattering off the extreme wings of atomic hydrogen lines. In the latter case, photons incident upon a neutral hydrogen slab are scattered monochromatically off the extreme damping wings of (mainly) Lyα λ1216, with a cross section for interaction similar to that which makes the Earth's day sky blue (Gavrila 1967; Mihalas 1978). The pure scattering albedo is 1 near 1200 Å for neutral hydrogen column densities exceeding $\sim 10^{20}$ cm^{-2}. We shall associate the Rayleigh scattering feature with the wavelength 1200 Å to distinguish it from the emission line Lyα λ1216.

The dominant sources of absorption opacity that most affect the UV-optical albedo of the broad-line clouds are bound-free transitions of the neutral and singly ionized species generally residing behind the hydrogen ionization front. Foremost among these is atomic hydrogen opacity in the various continua (Lyman, Balmer, Paschen, etc). Photoionization from excited states of He and He$^+$ is also important. Next in importance are the ionization edges of the more abundant atoms and singly ionized species of C, N, O, Mg, Si, S, Ca, Fe, ionized from the ground and in some cases the excited states. At large enough neutral hydrogen column densities, the opacities of the atoms of even the less abundant elements (e.g., Na, Al, P, K, Cr, Mn, Co, Ni) become significant. (The lightest 30 elements are included in the calculations; here we assume solar abundances of these elements [Grevesse & Anders 1989; Grevesse & Noels 1993]).

2.2. *Reflection from Broad-Line Clouds*

For a cloud of total column density N(H) and density n(H), the ionization parameter $U(\mathrm{H}) \equiv \Phi(\mathrm{H})/n(\mathrm{H})c$ mainly sets (1) the ionized hydrogen column density $N(\mathrm{H}^+)$ and thus the electron scattering albedo, (2) the neutral hydrogen column density $N(\mathrm{H}^0)$ and thus the Rayleigh scattering albedo and the hydrogen opacity, and (3) the opacities of the neutral and singly ionized metals. Thus N(H) and U(H), for a given incident continuum shape and chemical abundances, will determine the effective albedo of a BLR cloud. We assume a total hydrogen particle density of 10^{11} cm^{-3}, an incident optical–extreme ultraviolet (EUV) continuum of the form $f_\nu \propto \nu^{-1.2}$ exp $(-E/415$ eV) with an X-ray power law of the form $f_\nu \propto \nu^{-0.9}$ spanning 13.6–100 keV, and an $\alpha_{ox} = 1.2$. This SED may be appropriate for some Seyfert 1 galaxies (Walter et al. 1994). The choice of continuum shape does not strongly influence the general results presented here; however, different chemical abundances would have a significant impact on the effective albedo. The impact of gas density will be discussed. We used the spectral synthesis code CLOUDY, version 90.04 (Ferland 1996) assuming constant-density, plane-parallel slabs.

In Figures 2*a* and 2*b* we plot the effective UV-optical (800 Å–1.0 μm) albedo $[A_{\mathrm{eff}}(\lambda)]$ of BLR clouds for a range of cloud parameters U(H) and $N(\mathrm{H}^0)$, thought typical for the BLR. The effects of the hydrogen opacity and, in some cases, the metal opacity are clearly visible. Unless the Thomson optical depth is significant, $A_{\mathrm{eff}}(\lambda)$ is small except in the vicinity of 1200 Å and vanishes below the Lyman limit at 912 Å. The strength and breadth of the Lyα Rayleigh scattering feature is striking. We now discuss some of the important features of Figure 2.

The effective albedo for five neutral hydrogen column density clouds (10^{20}–10^{25} cm^{-2}) with log U(H) $= -2$ are plotted as light solid lines in Figure 2*a*. Note the increasing width and strength of the Rayleigh scattering feature with increasing $N(\mathrm{H}^0)$. For all but the smallest $N(\mathrm{H}^0)$ considered (10^{20} cm^{-2}), the $A_{\mathrm{eff}}(\lambda)$ is nearly 1 at 1200 Å. The electron scattering optical depth increases from essentially zero to 0.196, from small to large column density clouds. However, note that the corresponding albedo is never realized outside the reaches of the Lyα Rayleigh scattering profile. The reason for this is the gas bound-free opacity that also increases with column density. Under these conditions of relatively low ionization, the effective albedo is significant mainly in the spectral regions dominated by the Rayleigh scattering. Increasing the neutral column density beyond 10^{25} cm^{-2} does not increase the effective albedo significantly, since at these large neutral column densities the gas absorption opacity completely dominates over the scattering.

While most calculations of broad-line clouds assume thermal velocity fields, including these thus far, significant microturbulent or flow velocities may be present. If present, the effective albedo of the cloud can be altered by changes in the gas opacity; lower optical depths for Lyα and the excited state transitions of hydrogen (and helium) will reduce line trapping and hence the importance of photoionization from the excited states of hydrogen (and helium). Thus, the Thomson scattering optical depth will be diminished because of the reduced ionized hydrogen column density. For the same reason the Balmer continuum optical depth will also be reduced, as will optical depths of other excited state continua of H and He. Furthermore, the reduced excited state H, He opacities are compensated by increased photoionization of C^0 and neutral third and fourth row elements. Thus for sufficient column densities [i.e., log $N(\mathrm{H}^0) \gtrsim 24$], the effective albedo of the Rayleigh scattering feature can increase dramatically in the presence of microturbulence or in the presence of Sobolev velocity gradients, for reasons given above. Compare the bold solid line in Figure 2*a*, with a microturbulent velocity of $v_{\mathrm{turb}} =$ 100 km s^{-1}, with its counterpart from thermal width gas.

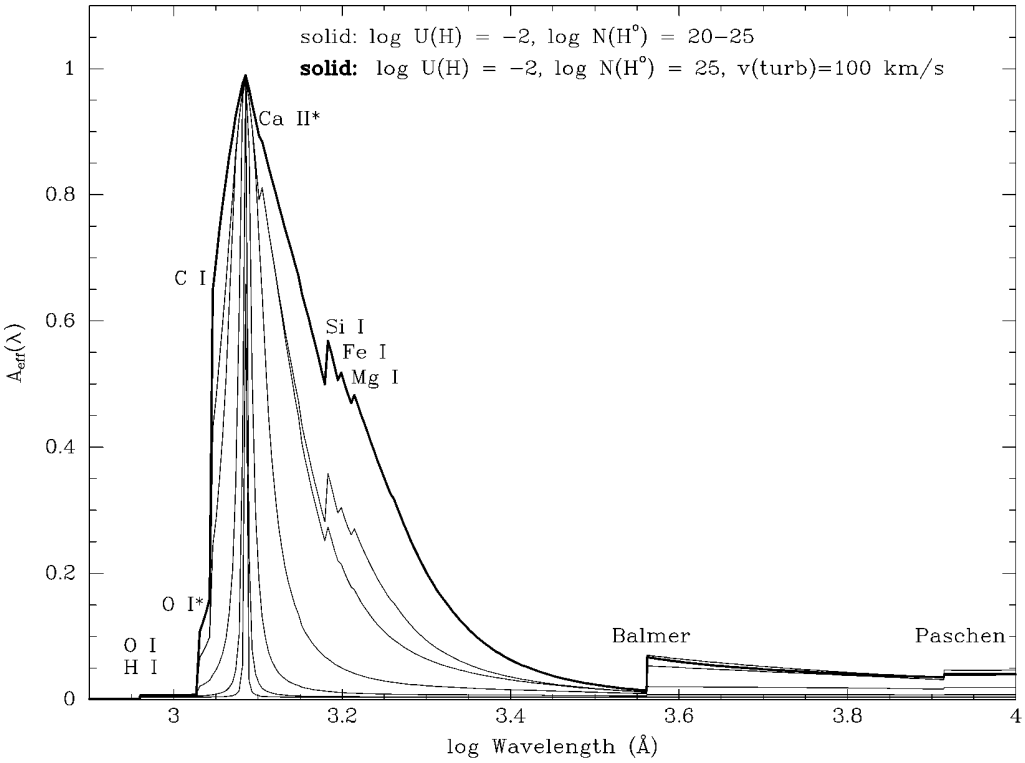

FIG. 2*a*

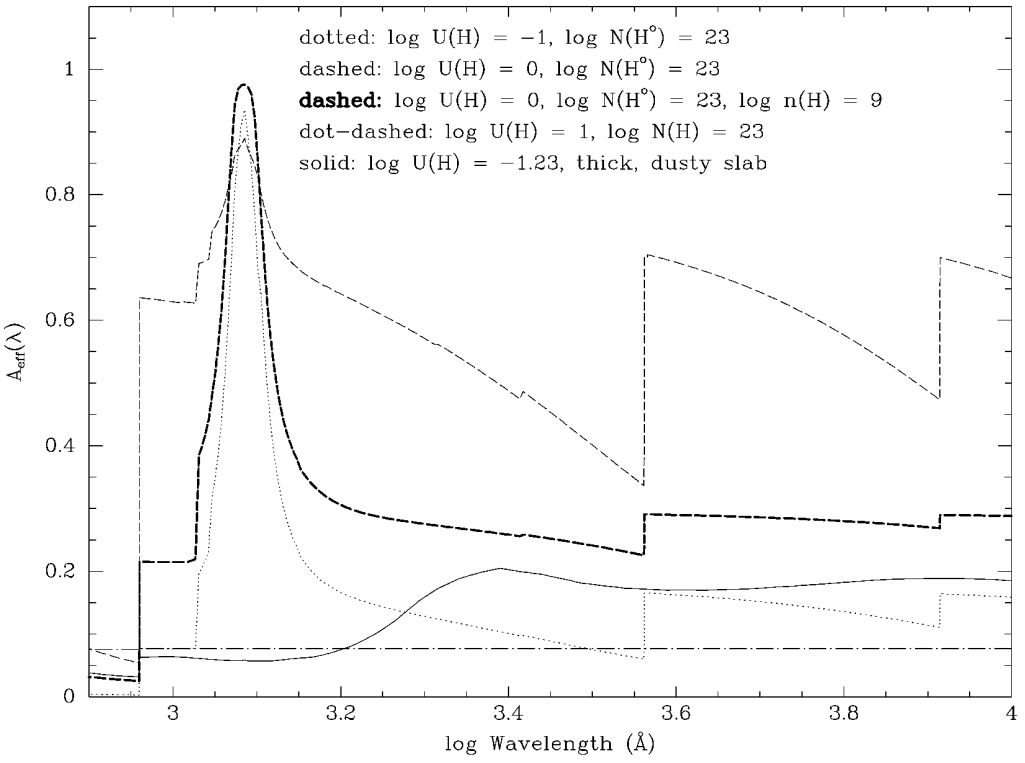

FIG. 2*b*

FIG. 2.—(*a*) Optical-UV effective continuum albedo as a function of log λ (Å) for clouds with a range in $N(H^0)$ and $U(H) = 0.01$, as labeled in the plot. Significant gas absorption opacity features are labeled. The bold curve includes the effects of introducing a turbulent velocity field with $\sigma = 100$ km s^{-1}. (*b*) Optical-UV effective continuum albedo as a function of log λ (Å) for a variety of cloud parameters, as labeled in the plot. The dot-dashed line represents the albedo of a matter-bounded cloud whose *total* column density is 10^{23} cm^{-2}. The solid line shows the effective albedo of a dusty, high column density cloud, $N(H^0) \approx 10^{25}$ cm^{-2}.

At larger ionization parameters, the gas becomes more ionized, and the importance of Thomson scattering to the albedo increases. $A_{\rm eff}(\lambda)$ is plotted as a dotted line in Figure 2*b* for log $N(\rm H^0) = 23$ and an ionization parameter of log $U(\rm H) = -1$. This curve should be compared to those for log $U(\rm H) = -2$ and log $N(\rm H^0) = 23$ and log $\rm N(H^\circ) = 25$, the third largest and largest $A_{\rm eff}(\lambda)$ plotted as solid lines in Figure 2*a* (with $v_{\rm turb} = 0$). In the first case the two clouds have the same $N(\rm H^0)$, but different ionization parameters. The cloud with the larger ionization parameter has a larger Thomson optical depth, and thus a larger albedo across most of the spectrum. In the second case the clouds have nearly the same Thomson optical depth (0.201 vs. 0.196); however, one of the clouds has 100 times the neutral hydrogen column density and thus a much stronger (i.e., broader) Rayleigh scattering feature. The larger $N(\rm H^0)$ cloud also has a much larger gas opacity; thus, its effective albedo falls below that of the lower column density, higher U(H) cloud for wavelengths longer than $\sim$1860 Å.

The light dashed line in Figure 2*b* is $A_{\rm eff}(\lambda)$ for log $N(\rm H^0) = 23$ and an ionization parameter of log $U(\rm H) = 0$, and should be compared to the effective albedos of the other clouds with log $N(\rm H^0) = 23$, but lower U(H). A cloud with large U(H) and column density will have a significant Thomson scattering optical depth, here $\tau_{\rm T} = 1.47$. Note the small but significant $A_{\rm eff}(\lambda)$ at wavelengths just longward of the Lyman limit. Even near 1200 Å, about 75% of $A_{\rm eff}(\lambda)$ is due to electron scattering, unlike the lower ionization clouds. However, the typical UV-optical $A_{\rm eff}(\lambda)$ outside the realm of the Rayleigh scattering feature is still less than the Thomson scattering albedo mainly because of the hydrogen absorption opacity. Note, too, that $A_{\rm eff}(\lambda 1200)$ is smaller (0.89) than for the previous clouds, since the opacities in the hydrogen Balmer and He I $2\ ^3S$ continua are significant enough to reduce the albedo here.

A broad range in gas densities is likely present in the BLR (Baldwin et al. 1995). Until now we have considered clouds with $n(\rm H) = 10^{11}$ cm^{-3}. At lower densities, e.g., $n(\rm H) = 10^9$ cm^{-3}, the flux in radiation at the illuminated face of the cloud is smaller at the same ionization parameter; thus, the atoms and ions have smaller excited state populations. In the case of hydrogen (the major electron donor and opacity source), this has three effects: (1) photoionization from excited states and collisional ionization becomes less important and the gas is less ionized, lowering the Thomson scattering albedo, (2) the recombination continua optical depths (e.g., Balmer) become smaller, so the drop in effective albedo shortward of the continuum edges is less pronounced, and (3) both of the foregoing effects result in a stronger Rayleigh scattering feature at a fixed $N(\rm H^0)$ and U(H). These differences are illustrated in Figure 2*b*, comparing the two dashed lines.

The effective albedo of a matter-bounded cloud is represented by the dot-dashed line in Figure 2*b* [$n(\rm H) = 10^{11}$ cm^{-3}, $U(\rm H) = 10$, total hydrogen column density $N(\rm H) = 10^{23}$ cm^{-2}]. The effective albedo is grey as expected, and for this cloud this characteristic extends between about 500 eV and 200 μm. At higher energies metal opacities alter the effective albedo, and at wavelengths longer than 200 μm, the free-free opacity does the same thing. If the column density were larger at this ionization parameter, the grayness limits at both ends would move toward the UV-optical regime. The free-free opacity will be larger for larger gas densities. Under most conditions, however, the $A_{\rm eff}$(800–912 Å) of a matter-bounded cloud will remain gray with increasing total column density at constant U(H) until the optical depth at 912 Å approaches unity [$N(\rm H^0) \sim 10^{17.2}$ cm^{-2}]; the $A_{\rm eff}$(912 Å-1 μm) will remain gray until a hydrogen ionization front forms [$N(\rm H) \gtrsim 10^{23.1}$ cm$^{-2} \times U(\rm H)$].

Finally, except from clouds with small $N(\rm H^0)$, the Rayleigh scattering feature does not have a symmetric profile. With increasing $N(\rm H^0)$, the feature broadens, but the short wavelength side of the profile is cut off by the ionization of C I, excited state O I, and then ground-state hydrogen and neutral oxygen at 912 Å. For $N(\rm H^0)$ approaching 10^{24} cm^{-2}, the ionization of excited state Ca II (near 1260 Å), ground-state Si I, Mg I, and Fe I (1500–1650 Å) reduces the albedo on the long-wavelength side of the Rayleigh scattering profile. These opacity features are labeled in Figure 2*a*.

2.3. *Reflection from Dusty, High Column Density Gas*

For purposes of comparison, we have plotted in Figure 2*b* (*solid line*) the $A_{\rm eff}(\lambda)$ from a high column density [log $N(\rm H) \approx 25$], dusty slab. The gas and grain abundances were assumed to approximate that of the Orion Nebula (Baldwin et al. 1996). The grains used here tend to be larger and thus more gray (the ratio of total to selective extinction is $R_V = 5.5$) in their optical properties than those of the diffuse Galactic ISM. The larger grain size distribution might be more appropriate for the AGN environment if we are observing gas that was just exposed from a molecular cloud. The hydrogen particle density was taken to be 10^8 cm^{-3}; the flux in hydrogen ionizing photons was set to $10^{17.25}$ s^{-1} cm^{-2}, just at the threshold for the sublimation of silicate grains. The corresponding ionization parameter was log $U(\rm H) = -1.23$. This was meant to be grossly representative of the obscuring dusty torus (e.g., Pier & Voit 1995), though the effective albedo of dusty gas depends little upon these latter details. The effective albedo is roughly flat over much of the optical-UV, and reaches values no larger than about 0.2. The dust albedo diminishes substantially below 2500 Å and above 1 μm. This is because, in our treatment, we discount forward scattering so the grains become good absorbers at long and short wavelengths. Other grain compositions and size distributions will have albedos whose spectral shapes may differ but whose overall amplitudes will not. It is notable that the dusty gas cloud of low Thomson optical depth (0.051) has a nonzero effective albedo at the Lyman limit (0.032), reaches a maximum of 0.052 near 1.54 ryd, and declines at higher energies. The Lyα Rayleigh scattering component is usually very weak or absent because of the large grain opacity. While the dusty cloud albedo never gets very high, it can compete with and even dominate over the BLR gas albedo longward of 2000 Å if the ratio of continuum source covering fractions (and so visibility) favors the dusty gas. This is discussed in the next section.

3. DISCUSSION

3.1. *The Integrated BLR Albedo*

The integrated BLR albedo is to first order a sum over each cloud's $A_{\rm eff}(\lambda) \times f_c$, where f_c is that cloud's covering fraction as seen by the continuum source. Of course, only those clouds whose illuminated sides are observable will contribute to the observed integrated BLR albedo. We can

expect that this corresponds to roughly one-half of the integrated cloud covering fraction, on average. We also expect that clouds with a broad range in properties will contribute to the integrated BLR albedo, rather than just the few types illustrated here. The shapes of clouds, their distribution in space, and viewer orientation will also play roles. We will not consider these complications here.

It is apparent from Figure 2 that clouds with significant Thomson optical depths, especially fully ionized ones, will contribute most to the integrated BLR albedo at all wavelengths except in the vicinity of Lyα. In the spectral region 1200 ± 200 Å a wide variety of ionization-bounded clouds of lower ionization parameter will contribute most to the integrated albedo. Next to the albedo in importance to the Rayleigh scattering component in ionization-bounded clouds are those spectral regions just to the long-wavelength sides of the various hydrogen recombination continuum edges, where the photoelectric absorption and diffuse emission are at their minima. Thus continuum photons scattering off broad-line clouds could alter the shapes of the spectral features near the Paschen, Balmer, and Lyman jumps, reducing the contrast at the continuum head. The effect would be largest for a population of high column density clouds with significant Thomson scattering optical depths. For the model represented by the light dashed line in Figure 2*b*, the scattered continuum photons represent 73% of the total light emitted at 3649 Å from the illuminated face of the cloud. However, unless the Thomson optical depth is significant, the diffuse emission from most clouds will dominate the reflected incident continuum, except in the vicinity of Lyα. While the contrast of either the diffuse emission or the scattered continuum to the central continuum flux in our direction would be expected to depend on the observer orientation and the spatial distribution of clouds, to first order their ratio $F_{\rm scat}/F_{\rm diff}$ integrated over the BLR would remain approximately invariant to these factors, since contributions to both of these quantities are emitted by the same entities. However, $F_{\rm diff}$ can also be emitted from the back sides of clouds, whose front sides are unviewable, and exact radiative transfer through nonslab clouds could also alter the predicted ratio.

The putative obscuring dusty torus likely covers a substantial portion of the sky as seen from the central continuum source and BLR, and could thus contribute significantly to the nuclear reflection spectrum in AGNs, even when the central continuum source is visible. The ratio of the covering fraction of the torus to that of the broad-line clouds likely ranges from roughly 1 to 5 (e.g., Pier & Krolik 1993), which means that the integrated albedo of a molecular torus could be competitive with or dominate over the BLR gas albedo longward of ~ 2000 Å, though the ratio of their *observable* emitting-reflecting surfaces is not likely to be simply the ratio of their covering fractions. In addition to the smooth incident continuum, the torus would also reflect the diffuse emission from the broad-line clouds. However, longward of 1 μm the dust reemission will overwhelm the reflected light from the continuum/BLR.

In summary, the integrated effective albedo over much of the UV-optical regime for the combined BLR plus torus mirrors should be a few to several percent, or higher if the electron scattering albedo is significant in the BLR. In the wavelength range 1130–1330 Å, the Rayleigh scattering feature will likely dominate the observable integrated effective albedo that could be as much as a few tens of percent.

3.2. *Rayleigh Scattering Contribution to the Observed Lyα Emission*

The Rayleigh scattering Lyα feature is the most significant source of albedo from ionization-bounded broad-line clouds. From variability studies (Clavel et al. 1991; Peterson et al. 1991; Korista et al. 1995), we infer the existence of ionization-bounded clouds of high column densities [$\log N({\rm H}) \gtrsim 10^{23}$ cm^{-2}]. Many of these must have substantial $N({\rm H}^0)$. Thus, if the UV-optical albedo of broad line clouds is important anywhere in the spectrum, it should be in the vicinity of Lyα. Figure 2 shows features that range in width from tens to hundreds of angstroms, much like the observed broad emission line profiles of Lyα. Might some fraction of the observed equivalent width (W_λ) of Lyα be a result of continuum Rayleigh scattering off the neutral portions of the broad line clouds?

In Figure 3 we plot the continuum normalized mean Lyα profile of NGC 5548, a Seyfert 1 galaxy, from the *Hubble Space Telescope* (*HST*) monitoring campaign of 1993 (Korista et al. 1995). Also plotted is the function $F_\lambda = 1 + A_{\rm eff}(\lambda) \times 0.5 f_c$, normalized at 1000 Å for three cloud covering fractions (0.1, 0.25, and 0.5), for clouds with $\log U({\rm H}) = -2$, $\log N({\rm H}^0) = 23$ (*dotted lines*). The factor of 0.5 in front of the covering fraction assumes that this is the fraction of clouds whose front faces are observable on average. The observable equivalent width of the Lyα Rayleigh scattering feature for clouds of these parameters is $W_{\lambda 1200}({\rm Rayleigh}) \approx 100$ Å $\times 0.5 f_c$, as measured between 1150 and 1300 Å, over which one might attempt to measure the strength of Lyα. For the effective albedo of this type of cloud, a maximum covering fraction of $\lesssim 0.5$ is allowed, corresponding to an observable $W_{\lambda 1200}({\rm Rayleigh}) \lesssim 25$ Å. This feature is very broad (FWHM $\approx 23{,}000$ km s^{-1}), and one of this strength may account for the extremely broad wings observed in Lyα (e.g., Zheng 1992) and the "shelf" upon which O I λ1304 and C II λ1335 appear to sit.

Clouds with smaller $N({\rm H}^0)$ will have narrower Rayleigh scattering profiles and smaller equivalent widths at a given covering fraction. For comparison, the Rayleigh scattering profile of a cloud with $\log U({\rm H}) = -2$, $\log N({\rm H}^0) = 22$ for $0.5 f_c = 0.25$ is plotted as a dashed line. Its observable equivalent width is $W_{\lambda 1200}({\rm Rayleigh}) \approx 40$ Å $\times 0.5 f_c$, while its FWHM is about 8800 km s^{-1}. Clouds with $\log N({\rm H}^0) \lesssim 22$ will not contribute significantly to the measured *line* emission at Lyα. The same is true for clouds with neutral hydrogen column densities greatly in excess of 10^{23} cm^{-2}, since the reflection profile will be too broad to measure as an emission-line feature.

Since the BLR is composed of clouds with a variety of $U({\rm H})$ and neutral column densities, and since a scattered light spectrum is always dependent upon the geometry, an upper limit to the contribution of Rayleigh scattering to the measured Lyα emission-line strength is not simple to predict, though a 10 Å equivalent width contribution is a reasonable expectation. A significant contribution would exacerbate the well-known Lyα/Hβ problem, described recently in Netzer et al. (1995).

3.3. *Reflection of Optical-UV Photons from Thick "Neutral" Media*

It should be obvious from Figure 2 that fully ionized gas of large column densities, whether broad line clouds or atmospheres of accretion disks, are not the only "mirrors" available in the vicinity of the central engine of an AGN.

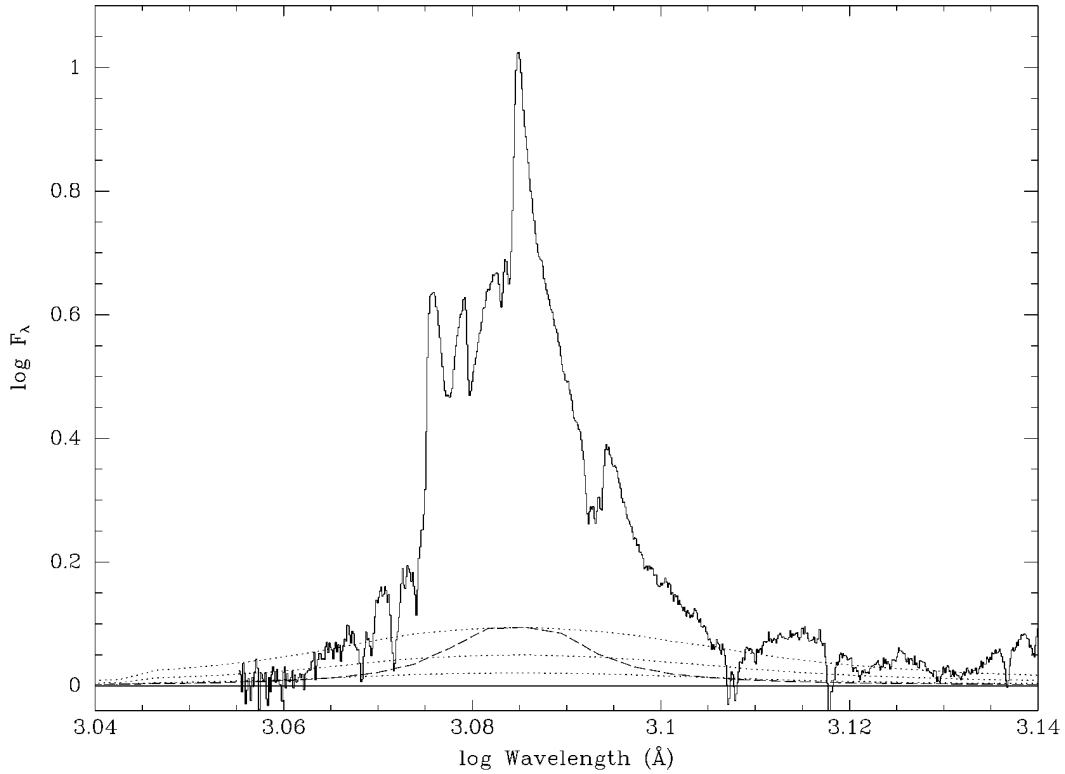

FIG. 3.—*Solid line*: Continuum normalized mean 1993 *HST* spectrum of NGC 5548. *Dotted lines*: Function $1 + A_{\rm eff}(\lambda) \times 0.5f_c$, normalized at 1000 Å for three cloud covering fractions (0.1, 0.25, and 0.5). The effective albedo is from a cloud with log U(H) = −2 and log $N(\rm H^0)$ = 23. *Dashed line*: Same function from a cloud with log $N(\rm H^0)$ = 22 and $0.5f_c = 0.25$. Geocoronal Lyα contaminates the blue midwing of the Lyα emission profile of NGC 5548. Note that both axes are on a $\log_{10}$ scale.

Any source of significant $N(\rm H^0)$ will reflect continuum and line photons over many tens or hundreds of angstroms near 1200 Å. Perhaps the broad-line clouds are not the most likely candidates for the very large neutral column density clouds ($>10^{24}$ cm^{-2}), but an accretion disk might be. As long as the cool, relatively neutral portions of the accretion disk do not contain dust and are not encased in an optically thick corona, then Rayleigh scattering would be expected to contribute significantly to the disk albedo in the UV. A glance at the heavy solid line in Figure 2*a* shows that this Rayleigh scattering mirror could be 30% to nearly 100% reflective over a ~700 Å span. Inwardly directed line photons that hit this gas would be reflected; most of the UV emission lines would be affected in this way to some degree (O VI λ1034 and Mg II λ2800 would be least affected). Lyα is expected to be affected the most, since it is beamed fully inward from ionization-bounded clouds (Ferland & Netzer 1979), and the effective disk albedo would be near unity near 1200 Å. For lines emitted near 1200 Å, such as N V λ1240, this effect is expected to be important even within broad-line clouds of lower neutral hydrogen column densities (see Fig. 2*a*).

If this highly reflective Rayleigh mirror exists, it would not be expected to lie in the inner portions of the accretion disk, where the gas temperature is $\gtrsim 10^5$ K and the neutral opacities are lower; electron scattering will dominate the albedo under these conditions. In addition to reflecting the inwardly streaming line photons, this warmer electron scattering mirror would broaden the line profile (line photons would retain their identity with the line as long as the temperature is less than about 10^6 K). Significant line and/or continuum emission scattered off the disk, whether by Rayleigh or electron scattering, could have an impact on the observed emission-line strengths, profiles, and line-continuum reverberation. For instance, might reflection off the disk symmetrize the Lyα emission-line profile? Figure 4 illustrates a possible scenario whereby radiation emitted by the illuminated face of a broad line cloud is redirected toward the observer via reflection off an accretion disk. Doppler shifts for clouds moving toward or away from the reflecting disk would have the opposite sign in reflection; Doppler motions parallel to the plane of the disk would remain approximately invariant to reflection. If the net

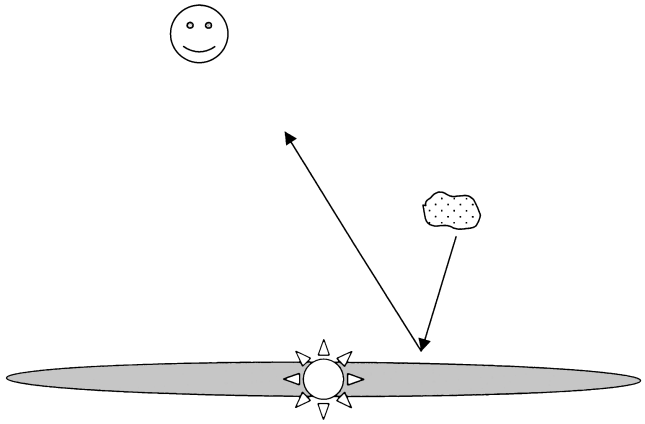

FIG. 4.—Cartoon illustrating the effect of an accretion disk reflecting inwardly directed emission from a broad-line cloud. The central ionizing source and the accretion disk are denoted by the star icon and shaded ellipse. Inwardly beamed radiation from the cloud, otherwise invisible to the observer, is reflected toward the smiling observer. Emission line clouds on the other side of the disk from the observer are invisible to the observer.

cloud motion were away from the disk, and toward the observer, the portion of Lyα that would be visible to the observer would have a net blueshift (clouds on the far side of the disk are blocked from view), in the absence of reflection from the disk. However, the inwardly beamed Lyα photons would be efficiently reflected from the disk and redirected toward the observer with the opposite Doppler shift.

Reflection off an accretion disk could solve a longstanding conundrum. Given the strength of the observed Balmer continuum, a Lyman jump in emission is also expected. However, none has ever been seen. The lack of a strong feature near 912 Å, whether in absorption (from the accretion disk?) or emission (from the broad-line clouds and/or accretion disk), has been a puzzle (Carswell & Ferland 1988; Antonucci et al. 1996). One way to destroy a Lyman jump in emission from broad-line clouds is to reflect it off a source of neutral hydrogen, perhaps the outer accretion disk, before we observe it.

3.4. *Scattered Light in Broad Absorption Line Troughs*

One of the motivations of this work was that recent high-quality spectropolarimetric observations of broad absorption line (BAL) QSOs have shown that the BAL troughs are filled substantially with scattered light (Glenn et al. 1994; Cohen et al. 1995; Goodrich & Miller 1995; Hines & Wills 1995; Goodrich 1997). The resonance line troughs in BAL QSOs are observed to be more polarized than the adjacent continuum. Investigators have proposed several scenarios, one of which suggests that we observe two continuum sources. The primary continuum is of little or no polarization and is seen directly through the BAL gas. The secondary continuum results from the scattering of primary continuum photons off some extended geometry into our line of sight, which takes a different path through the BAL resonance scattering region (Fig. 4 in Cohen et al. 1995). The total continuum is the sum of the two and we see the strongly polarized light ($P \approx 10\%$) only at the bottoms of the troughs where much of the primary, unpolarized continuum has been resonance-scattered from the line of sight. Some unknown fraction of the scattered light at the bottoms of the troughs is certain to be that from the scattering of the continuum by the resonance lines which form the troughs (Hamann, Korista, & Morris 1993; Hamann & Korista 1996; Lee & Blandford 1997), and possibly from dust or electron scattering within or interior to the BAL flow. But assuming the "extended secondary continuum" scenario to be correct, could some portion of the BLR contribute to its origin?

A significant fraction of those clouds emitting the broad emission lines must be covered by the BAL outflow (Turnshek et al. 1988). This is clear from the weakness of Lyα emission in many BAL QSOs as a result of scattering by the N^{+4} ions in the BAL outflow, and also from the observed C IV BAL profiles at lower outflow velocities. However, some fraction of the BLR might lie along sight lines of lower or zero optical depth through the BAL region and act as an extended continuum source. Is there a spectral signature in the observed scattered (polarized) light that we may identify as emerging from the BLR?

Figure 2 illustrates a wide variety of $A_{\rm eff}(\lambda)$ expected from BLR clouds. The albedo of BLR clouds in the UV results from some combination of Rayleigh plus electron scattering that is diminished by various atomic opacity sources. The wavelength dependence of the reflectivity of the BLR mirror could be as featureless as pure electron scattering or as "blue" as Rayleigh scattering, and is likely somewhere in between. A Keck spectropolarimetric observation of the high-redshift BAL QSO 0105−265 (Cohen et al. 1995) shows that the polarized light does not diminish or disappear abruptly at wavelengths shortward of 1100, 1064, and 912 Å as would be expected for the case of broad-line clouds with a significant $N(H^0)$. These types of clouds cannot dominate this mirror's composition. The most prominent sign of reflection by an ionization-bounded cloud of significant column density is the Rayleigh scattering feature. However, this has the misfortune of lying near the unpolarized broad Lyα emission line and is also susceptible to resonance line scattering by the the N V ion in the outflowing gas. Determination of the origin(s) of this scattered light will require disentangling the various possible sources of scattered light from each other and from sources that dilute the polarized light.

4. SUMMARY

We have explored the effective UV-optical albedos of a variety of possible broad emission line clouds, as well as their effects on the observed spectra of AGNs. The effective albedo results from an interplay between the scattering and absorption opacities. In moderately ionized ionization-bounded clouds the most important source of albedo is that which is due to Rayleigh scattering of continuum photons off the extreme damping wings of Lyα. The photons resulting from this scattering mechanism may contribute significantly to the Lyα emission line, especially in the very broad wings. Broad-line clouds with $N(H^0) \gtrsim 10^{21}$ cm^{-2} will reflect an increasingly significant fraction of the N V λ1240 photons that stream toward the neutral portion of the cloud. Other emission lines may be similarly affected to differing degrees. Inclusion of this effect can alter predicted emission-line strengths and profiles because the line beaming function becomes more anisotropic. The effective albedo from a significant population of highly ionized, ionization-bounded clouds arises from Thomson scattering, and is diminished by the neutral hydrogen opacity. The interesting feature here is that the effective albedo tends to be a maximum just *longward* of the continuum edges. Thus a significant albedo from such clouds could alter the shape of the spectrum near the Balmer jump, for example. Fully ionized clouds will have nearly gray, Thomson scattering, UV-optical albedos. A thick, dusty cloud will contribute a fairly gray near-UV to optical albedo. In the absence of a strong Thomson scattering mirror, the dusty torus could dominate the albedo from the nuclear regions longward of ∼2000 Å due as a result of the torus' expected large covering fraction. The accretion disk may act as electron and Rayleigh scattering mirrors of broad emission line photons as well as central continuum photons, but its impact on the observed UV-optical spectrum of quasars awaits a fuller understanding of the accretion phenomenon. Finally, ionization-bounded BLR clouds may be a contributor to the mirror proposed to explain the polarized BAL troughs.

This work was supported by NASA grant NAG-3223 and NSF grant AST 96-17083. We thank Bob Goodrich and Patrick Ogle for helpful discussions, and we are grateful to an anonymous referee for his or her constructive comments.

REFERENCES

Antonucci, R. R. J., Geller, R., Goodrich, R. W., & Miller, J. S. 1996, ApJ, 472, 502
Antonucci, R. R. J., & Miller, J. S. 1985, ApJ, 297, 621
Baldwin, J. A., Ferland, G. J., Korista, K. T., & Verner, D. A. 1995, ApJ, 455, L119
Baldwin, J. A., et al. 1996, ApJ, 468, L115
Carswell, R. F., & Ferland, G. J. 1988, MNRAS, 235, 1121
Clavel, J., et al. 1991, ApJ, 366, 64
Cohen, M. H., Ogle, P. M., Tran, H. D., Vermeulen, R. C., Miller, J. S., Goodrich, R. W., & Martel, A. R. 1995, ApJ, 448, L77
Ferland, G. J. 1996, in Hazy, Univ. Kentucky Dept. Phys. and Astron. Internal Rep.
Ferland, G. J., & Netzer, H. 1979, ApJ, 229, 274
Gavrila, M. 1967, Phys. Rev., 163, 147
Glenn, J., Schmidt, G. D., & Foltz, C. B. 1994, ApJ, 434, L47
Goodrich, R. W. 1997, ApJ, 474, 606
Goodrich, R. W., & Miller, J. S. 1994, ApJ, 434, 82
———. 1995, ApJ, 448, L73
Grevesse, N., & Anders, E. 1989, in AIP Conf. Proc. 183, Cosmic Abundances of Matter, ed. C. J. Waddington (New York: AIP), 1
Grevesse, N., & Noels, A. 1993, in Origin and Evolution of the Elements, ed. N. Prantzos, E. Vangioni-Flam, & M. Casse (Cambridge: Cambridge Univ. Press), 15
Hamann, F., & Korista, K. T. 1996, ApJ, 464, 158
Hamann, F., Korista, K. T., & Morris, S. L. 1993, ApJ, 415, 541
Hines, D. C., & Wills, B. J. 1995, ApJ, 448, L69
Koratkar, A., Antonucci, R. R. J., Goodrich, R. W., Bushouse, H., & Kinney, A. L. 1995, ApJ, 450, 501
Korista, K. T., et al. 1995, ApJS, 97, 285
Krolik, J. H., Madau, P., & Życki, P. T. 1994, ApJ, 420, L57
Lee, H.-W., & Blandford, R. D. 1997, MNRAS, 288, 19
Lightman, A. P., & White, T. R. 1988, ApJ, 335, 57
Mihalas, D. 1978, Stellar Atmospheres (2d ed.; San Francisco: Freeman)
Miller, J. S., & Antonucci, R. R. J. 1983, ApJ, 271, L7
Miller, J. S., & Goodrich, R. W. 1990, ApJ, 355, 456
Nandra, K., & George, I. M. 1994, MNRAS, 267, 974
Netzer, H., Brotherton, M. S., Wills, B. J., Han, M., Wills, D., Baldwin, J. A., Ferland, G. J., & Brown, I. W. A. 1995, ApJ, 448, 27
Peterson, B. M., et al. 1991, ApJ, 368, 119
Pier, E. A., & Krolik, J. H. 1993, ApJ, 418, 673
Pier, E. A., & Voit, G. M. 1995, ApJ, 450, 628
Poutanen, J., Sikora, M., Begelman, M. C., & Magdziarz, P. 1996, ApJ, 465, L107
Ross, R. R., & Fabian, A. C. 1993, MNRAS, 261, 74
Tran, H. D., Miller, J. S., & Kay, L. E. 1992, ApJ, 397, 452
Turnshek, D. A., Foltz, C. B., Grillmair, C. J., & Weymann, R. J. 1988, ApJ, 325, 651
Walter, R., Orr, A., Courvoisier, T. J.-L., Fink, H. H., Makino, F., Otani, C., & Wamsteker, W. 1994, A&A, 285, 119
Zheng, W. 1992, ApJ, 385, 127
Życki, P. T., Krolik, J. H., Zdziarski, A., & Kallman, T. R. 1994, ApJ, 437, 597